Comparison of a statistical model for magnetic islands in large current layers with Hall MHD simulations and Cluster FTE observations

R. L. Fermo,[1] J. F. Drake,[1] M. Swisdak,[1] and K.-J. Hwang[2,3]

Received 8 November 2010; revised 17 June 2011; accepted 5 July 2011; published 24 September 2011.

[1] Magnetic islands have been observed in long current layers for various space plasmas, including the magnetopause and solar corona. In previous work exploring these magnetic islands, a statistical model was developed that described their formation, growth, convection, and coalescence in very large systems, for which simulations prove inadequate. An integro-differential equation was derived for the island distribution function, which characterized islands by the flux they contain ψ and the cross-sectional area they enclose A. The steady-state solution of the evolution equation predicted a distribution of islands. Here, we use a Hall MHD (magnetohydrodynamic) simulation of a very long current sheet with large numbers of magnetic islands to explore their dynamics, specifically their growth via two distinct mechanisms: quasi-steady reconnection and merging. We then use the simulation to validate the statistical model and benchmark its parameters. A database of 1,098 flux transfer events (FTEs) observed by Cluster between 2001 and 2003 is also compared with the model's predictions. In both simulations and observations, island merging plays a significant role. This suggests that the magnetopause is populated by many FTEs too small to be recognized by spacecraft instrumentation.

Citation: Fermo, R. L., J. F. Drake, M. Swisdak, and K.-J. Hwang (2011), Comparison of a statistical model for magnetic islands in large current layers with Hall MHD simulations and Cluster FTE observations, *J. Geophys. Res.*, *116*, A09226, doi:10.1029/2010JA016271.

1. Introduction

[2] Magnetic reconnection is an important mechanism by which magnetic energy is transformed into plasma flows and particle energization in various space and astrophysical plasmas. Recent attention in magnetic reconnection research has focused on magnetic islands (also called plasmoids in some literature), a natural consequence of the tearing instability [*Furth et al.*, 1963]. Secondary magnetic islands have been seen in particle-in-cell (PIC) simulations of elongated current sheets, where reconnection becomes bursty when a guide field is introduced [*Drake et al.*, 2006a]. The electron current layer lengthens in the vicinity of the x-line and becomes unstable to the formation of secondary islands, which in turn grow and merge with one another. Plasmoid formation has been seen in numerous other kinetic simulations even without a guide field [*Daughton et al.*, 2006; *Fujimoto*, 2006; *Karimabadi et al.*, 2007; *Klimas et al.*, 2008; *Daughton et al.*, 2009], and also in MHD simulations for sufficiently high Lundquist number $S = Lc_A/\eta$ (where L is a length scale comparable to the system size, c_A is the upstream Alfvén speed, and η is the resistivity) [*Biskamp*, 1986; *Lapenta*, 2008; *Samtaney et al.*, 2009; *Cassak et al.*, 2009; *Huang and Bhattacharjee*, 2010].

[3] There also exists a great deal of observational evidence for magnetic islands, which in a 3D picture take the form of flux ropes. The patchy nature of reconnection has been supported by early satellite observations at the magnetopause, where these flux ropes take the form of flux transfer events (FTEs) [*Russell and Elphic*, 1978; *Lee and Fu*, 1985; *Farrugia et al.*, 1988]. More recently, similar plasmoid structures have also been observed in the magnetotail [*Elphic et al.*, 1986; *Slavin et al.*, 1993, 2003; *Eastwood et al.*, 2007]. In coronal images of solar flares, tadpole-like downflowing structures have been interpreted as flux tubes associated with reconnection [*Sheeley et al.*, 2004; *Lin et al.*, 2005; *Linton and Longcope*, 2006].

[4] The recent interest in magnetic islands is in part due to a connection with particle energization and the possible enhancement of the effective reconnection rate. Simulations suggest that a first-order Fermi mechanism enables electron acceleration to very high energies within contracting islands [*Drake et al.*, 2006b]. Cluster observations of highly energetic electrons correlated with islands in the magnetotail support this theory [*Chen et al.*, 2008], although contrary observational data [*Egedal et al.*, 2010] illustrates that this remains an important and open question. A rescaling of

[1]Institute for Research in Electronics and Applied Physics, University of Maryland, College Park, Maryland, USA.
[2]Goddard Earth Sciences Technology Center, University of Maryland Baltimore County, Baltimore, Maryland, USA.
[3]NASA Goddard Space Flight Center, Greenbelt, Maryland, USA.

Copyright 2011 by the American Geophysical Union.
0148-0227/11/2010JA016271

Sweet-Parker reconnection that accounts for the presence of secondary islands also suggests that the reconnection rate could scale with the square root of the number of islands [*Cassak et al.*, 2009]. A linear MHD theory of the plasmoid instability predicts the number of islands to scale as $S^{3/8}$ [*Loureiro et al.*, 2007]. This theory is supported by MHD simulations by *Samtaney et al.* [2009], but only during the linear stage, before merging and plasmoid convection become important. One theory by *Huang and Bhattacharjee* [2010] suggests that in the nonlinear regime, plasmoids dominate until the effective Lundquist number for the shortened current sheet between plasmoids becomes small enough to suppress the plasmoid instability ($S_{local} < S_{crit} \approx 10^4$). Fully kinetic simulations that include a Fokker-Planck collision operator have also exhibited the plasmoid instability and enhanced reconnection rates as the current sheet thickness nears the ion skin depth $d_i = c/\omega_{pi} = (m_i c^2/4\pi n e^2)^{1/2}$ [*Daughton et al.*, 2009].

[5] A fundamental question concerning the dynamics of magnetic islands that are produced as a result of reconnection is how they develop from their birth at small spatial scales to macroscale objects. However, their dynamics in very long current layers is difficult to study using only simulations. Computational resources limit the ability of PIC simulations to reach scale sizes comparable to the systems in question ($L \sim 800 d_i$ for some of the largest 2D PIC simulations performed to date [*Daughton et al.*, 2009], but $L \sim 4000 d_i$ for the magnetopause and $L \sim 10^6 d_i$ for the solar corona). Global fluid simulations reach these scales [*Raeder*, 2006; *Dorelli and Bhattacharjee*, 2009], but might not capture the small-scale physics of reconnection and island formation. Resistive MHD simulations have explored the very early linear stage of the plasmoid instability [*Samtaney et al.*, 2009], but do not extend long enough in time to probe the long-term dynamics of plasmoids to large scales. Accordingly, an alternative approach is needed besides simulations. One such approach by *Uzdensky et al.* [2010] based on a model of fractal reconnection [*Shibata and Tanuma*, 2001] down to the scales where the plasmoid instability is suppressed [*Huang and Bhattacharjee*, 2010] predicts enhanced reconnection and a power law distribution of plasmoids. In this paper, we discuss another theoretical approach which has been developed whereby the magnetic islands are modeled statistically [*Fermo et al.*, 2010].

[6] Islands are born due to the tearing mode instability at wavelengths $2\pi/k$, with k the wavevector, such that $k\lambda \leq 1$, where λ is the characteristic transverse scale of the current layer supporting the reconnecting magnetic field. The linear tearing mode saturates at small amplitude when the island width is comparable to λ. From those small scales, two distinct mechanisms have previously been identified that allow islands to grow to macroscales. These mechanisms can be quantified by how the island gains flux and area. In the first, the island increases in size by quasi-steady reconnection on either end of the island, which causes both the area and flux of the island to increase together [*Fermo et al.*, 2010; *Uzdensky et al.*, 2010]. In the second, two islands can merge together into a single larger island [*Finn and Kaw*, 1977; *Pritchett and Wu*, 1979]. In this case, the area of the resultant island is the sum of the two areas, while its flux is equal to that of the island with the larger flux. The competition between these two distinct mechanisms for island growth balanced with convective loss ultimately controls the distribution of magnetic islands that develop in large scale current layers. Although the dynamics of magnetic islands have been investigated in preexisting literature (island formation [*Furth et al.*, 1963; *Loureiro et al.*, 2007], growth [*Hesse and Birn*, 1991; *Angelopoulos et al.*, 1995], convection [*Dailey et al.*, 1985; *Birn et al.*, 1996], coalescence [*Pritchett and Wu*, 1979; *Dorelli and Birn*, 2001]), only recently have these processes been studied together in a single model in the study by *Fermo et al.* [2010], where we derived an equation that describes the dynamics of these competing processes on a statistical basis. In the present manuscript we explore the competition between the two island growth mechanisms with Hall MHD simulations in a very long current layer, then test and benchmark our statistical model by comparing with the simulations. Finally, we compare the predictions of the statistical model with THEMIS observations of flux transfer events (FTEs) at the magnetopause.

2. Overview of the Statistical Model

[7] The model developed in the study by *Fermo et al.* [2010] considers magnetic islands forming in a current sheet with an equal and opposite reconnecting magnetic field B_0 on both sides. Islands generally grow at the reversal region and therefore develop like beads on a string. It assumes fast, patchy reconnection – fast compared to the convective time scales of plasma flow, and patchy enough to produce many magnetic islands along the current sheet. We then formulate a statistical distribution function f that characterizes magnetic islands by their magnetic flux ψ and their cross-sectional area A. Rather than simulating the whole domain of size L, f gives the number of magnetic islands in a current sheet with flux in the range $[\psi, \psi + d\psi]$ and area in $[A, A + dA]$ by the differential $dN = f(\psi, A)d\psi dA$. In this approach, an integro-differential equation for f is derived, analogous to the Boltzmann equation for the plasma distribution function. (*Uzdensky and Goodman* [2008] also use a similar approach to model magnetic loops in accretion disk coronae.) The evolution equation for f must include all of the dynamics of these islands observed in PIC simulations. The steady-state solution of this evolution equation would then predict the distribution of islands in the long current sheets found in space and astrophysical systems. This is not to say that the current sheet is itself at a steady-state. Rather, we suppose that the system after some time has reached a point where the distribution of islands is representative of the distribution at any other time.

[8] The complete evolution equation for f derived by *Fermo et al.* [2010] was

$$\begin{aligned}\frac{\partial f}{\partial t} + \frac{\partial}{\partial \psi}(\dot{\psi} f) + \frac{\partial}{\partial A}(\dot{A} f) &= S(\psi, A) - \frac{c_A}{L} f \\ &+ \frac{K_{mrg}}{L}\int_0^A dA' f(\psi, A')\int_0^\psi d\psi' \nu(\psi, A', \psi', A - A') f(\psi', A - A') \\ &- \frac{K_{mrg}}{L} f(\psi, A)\int_0^\infty dA' \int_0^\infty d\psi' \nu(\psi, A, \psi', A') f(\psi', A') \qquad (1)\end{aligned}$$

where

$$v^2(\psi_1, A_1, \psi_2, A_2) = \frac{\psi_1\psi_2 r_1 r_2 \left(r_1^2 + d_i^2\right)^{1/2}\left(r_2^2 + d_i^2\right)^{1/2}}{4\pi\rho\left(r_1^2 + d_e^2\right)^{3/2}\left(r_2^2 + d_e^2\right)^{3/2}} \quad (2)$$

is the merging velocity, $\dot{\psi} = \varepsilon c_A B_0$, and $\dot{A} = 2\varepsilon c_A\sqrt{\pi A}$ for a constant normalized reconnection rate ε. The two integral terms describe the probability of merging in some time Δt as proportional to $v\Delta t/L$. In the analogy with the Boltzmann equation, the merging terms play the role of the collision operator. For an incompressible plasma, when two islands (with, say, fluxes ψ_1 and $\psi_2 < \psi_1$ and areas A_1 and A_2) merge, the resultant island will have flux ψ_1 and area $A_1 + A_2$. This hypothesis was verified in PIC simulations [*Fermo et al.*, 2010] and is reflected in equation (1).

[9] The main features of the equation are: (1) the change in flux $\dot{\psi}$ and size $\dot{A}$ due to growth via quasi-steady reconnection, (2) the source term $S(\psi, A)$ that creates islands at small (down to d_e) scales, (3) a sink term allowing for the convection of islands out the side of the system at the rate c_A/L, and (4) the integral terms that describe the merging process. These are the four primary modes by which the distribution of islands changes. Our goal is to benchmark these mechanisms, and in particular the first and fourth, with Hall MHD simulations. Since the rate of merging is only an approximation, we have also introduced a new dimensionless coefficient to the merging terms, K_{mrg}. A value of $K_{mrg} = 1$ corresponds with the original equation derived in the study by *Fermo et al.* [2010], in which the form of the merging terms was hypothesized. We will infer a value for this coefficient by fitting it with the results of the Hall MHD simulations.

3. Hall MHD Simulations

[10] We use the Hall MHD code F3D [*Shay et al.*, 2004] to test this model against a simulated 2D current sheet of length $L \sim 1638.4d_i$. To this date, Hall MHD simulations of current sheets of this size have never before been used to explore the dynamics of many magnetic islands. It is worth noting, however, that the simulation is not a perfect replica of the systems in question, and is missing some of the dynamics that the statistical model includes. Nonetheless, it is useful in validating those aspects of the model that it does describe accurately, in particular the two mechanisms for island growth: quasi-steady reconnection and merging.

[11] For the first of these mechanisms, the growth of islands is governed by a normalized reconnection rate ε: the characteristic radius $r = \sqrt{A/\pi}$ increases at the rate $\dot{r} = \varepsilon c_A$ (where c_A is the Alfvén speed based on the reconnecting upstream magnetic field B_0) and the flux increases at the rate $\dot{\psi} = \varepsilon c_A B_0$. (Note that the characteristic radius r is used simply as a proxy for the more fundamental parameter A; the islands need not be round, and in fact are usually elongated.) In full particle-in-cell simulations of reconnection, after reaching a nonlinear stage, the normalized reconnection rate often plateaus at roughly $\varepsilon = 0.1$ [*Shay et al.*, 2007]. Although resistive MHD simulations do not show reconnection rates this fast, the inclusion of the Hall term has been shown to enable reconnection rates comparable to those including kinetic effects explicitly [*Birn et al.*, 2001]. Therefore, the Hall MHD simulations should describe accurately the island growth by quasi-steady reconnection in the system. With regards to the merging terms, although the incompressibility assumed by the model is not explicitly enforced by the code, in practice the density variations observed in Hall MHD simulations of reconnection do not appear to be strong enough to significantly alter the merging rules described in section 2.

[12] Unfortunately, the Hall MHD code is not as effective in modeling the source term $S(\psi, A)$. PIC simulations have shown that in reconnecting current layers, islands form and are convected out, leaving behind a thin, elongated current sheet that is again unstable to island formation. We therefore require $S(\psi, A)$ to generate islands continuously and at a steady rate [*Drake et al.*, 2006a]. This process does not occur naturally in these Hall MHD simulations of reconnection. MHD simulations generate magnetic islands spontaneously for sufficiently large values of the Lundquist number, $S \gtrsim 3 \times 10^4$ [*Biskamp*, 1986; *Bhattacharjee et al.*, 2009], but the onset of Hall reconnection during island formation sweeps away secondary islands, leaving a single large x-line [*Shepherd and Cassak*, 2010]. Instead, we initialize the current sheets with a small perturbation to the magnetic field. The perturbations (with wavelengths down to $L_x/256$) eventually grow into hundreds of islands. Although the simulation does not properly describe spontaneous secondary island formation, the islands which do form as a result of the initial perturbation are quite small, comparable in size with those generated by a tearing mode instability. Also, this Hall MHD simulation does not model the convective loss term of equation (1) because it employs periodic boundaries along the outflow. Periodicity is necessary because the simulation does not model island formation correctly yet, and it is preferable that the islands remain in the simulation domain for as long as possible since the goal of the simulations is to explore the growth and dynamics of large numbers of magnetic islands.

3.1. Computational Details

[13] The 2D simulations were performed using the compressible two-fluid code F3D, which solves the Hall MHD equations [*Shay et al.*, 2004]:

$$\frac{\partial n}{\partial t} = -\nabla \cdot \mathbf{J}_i \quad (3)$$

$$\frac{\partial \mathbf{J}_i}{\partial t} = -\nabla \cdot \frac{\mathbf{J}_i\mathbf{J}_i}{n} + \mathbf{J} \times \mathbf{B} - \frac{T}{n}\nabla n \quad (4)$$

$$\frac{\partial \mathbf{B}'}{\partial t} = -\nabla \times \mathbf{E}' \quad (5)$$

$$\mathbf{E}' = \frac{1}{n}\mathbf{J} \times \mathbf{B}' - \frac{1}{n}\mathbf{J}_i \times \mathbf{B} \quad (6)$$

$$\mathbf{B}' = \left(1 - d_e^2\nabla^2\right)\mathbf{B} \quad (7)$$

$$\mathbf{J} = \nabla \times \mathbf{B} \quad (8)$$

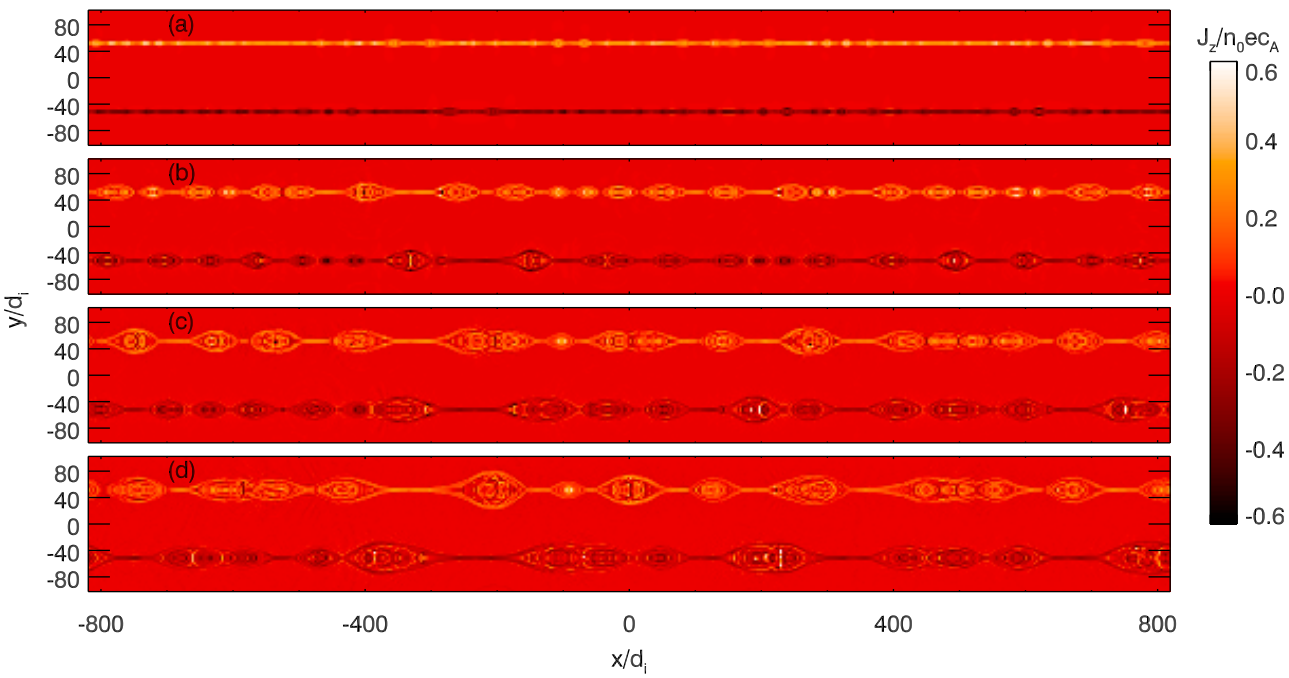

Figure 1. Snapshots of J_z in the Hall MHD simulation showing island formation, growth, and merging at (a) $t = 420\Omega_{ci}^{-1}$, (b) $t = 520\Omega_{ci}^{-1}$, (c) $t = 620\Omega_{ci}^{-1}$, and (d) $t = 686\Omega_{ci}^{-1}$. Values of J_z are capped at $J_z = \pm 0.6 n_0 e c_A$.

where $\mathbf{J}_i$ is the ion flux, $\mathbf{u}_e = (\mathbf{J}_i - \mathbf{J})/n$ the electron velocity, and $d_e = c/\omega_{pe}$ the electron skin depth. The mass ratio $m_e/m_i = 1/25$, and the grid scale is $0.1d_i$, enough to marginally resolve the electron skin depth $d_e = 0.2d_i$. The system size is $L_x \times L_y = 1638.4d_i \times 204.8d_i$ with periodic boundary conditions. Magnetic fields and densities are normalized to their asymptotic values far from the current sheets, B_0 and n_0 respectively. (Quasineutrality is assumed, so that $n_i \approx n_e$). Time is normalized to the ion cyclotron period, $t_0 = \Omega_i^{-1} = m_i c/eB_0$, length to the ion skin depth $L_0 = d_i = \sqrt{m_i c^2/4\pi n_0 e^2}$, velocity to the Alfvén velocity $v_0 = c_A = B_0/\sqrt{4\pi n_0 m_i}$, electric field to $E_0 = c_A B_0/c$, and temperature to $T_0 = m_i c_A^2$. The electron charge and ion mass are both normalized to 1.

[14] The initial configuration consists of double Harris sheets of width $w_0 = d_i$:

$$B_x \begin{cases} B_0 \tanh\left(\dfrac{y - 3L_y/4}{w_0}\right) & y < L_y/2 \\ -B_0 \tanh\left(\dfrac{y - L_y/4}{w_0}\right) & y > L_y/2 \end{cases} \tag{9}$$

There is no initial guide field ($B_z = 0$). The density at the center of the current sheets is $1.5n_0$ and falls to $1.0n_0$ to balance magnetic pressure. The initial configuration also includes a magnetic perturbation with wave numbers up to $k = (5/32)d_i^{-1}$. This perturbation acts as the seed for magnetic islands. The maximum k produces perturbations with wavelength $L_x/256$. This ensures that the each current sheet will produce $\gtrsim$100 islands, sufficient for a statistically significant analysis. The simulation includes neither viscosity nor resistivity explicitly, but does include a fourth-order diffusion term for B in Faraday's law, equation (5). The fourth-order diffusion coefficient is initially $2 \times 10^{-5}\ d_i^4\Omega_{ci}$ but later, in order to prevent grid-scale instabilities, is increased to $5 \times 10^{-5}\ d_i^4\Omega_{ci}$ after the islands have grown from the initial perturbation to a discernible size. The time step starts off as $\Delta t = 0.04\Omega_{ci}^{-1}$ but is adjusted to $\Delta t = 0.025\Omega_{ci}^{-1}$ at the time of the increase of the fourth-order diffusion coefficient.

3.2. Simulation Results and Analysis

[15] Figure 1 shows the time-evolution of this system. The initial perturbations grow into magnetic islands that undergo the dynamics described above. The islands begin as very small perturbations that first grow into discernible islands in Figure 1a. In Figure 1b these islands have reached scales large enough so that islands on a single layer interact with one another. The full merger of several islands is evident by Figure 1c. The final state of our simulation is shown in Figure 1d. Figure 2 shows the positions of all the o-lines in the lower current sheet in time. The convergence of two or more o-lines indicates the merging of those islands.

[16] An automated algorithm goes through successive frames of the simulation and tracks the size and flux of each of the magnetic islands in a particular current sheet. The tracking algorithm uses the flux function $\Psi(x, y)$ defined such that

$$\mathbf{B}(x,y) = \hat{\mathbf{z}} \times \nabla\Psi(x,y) + B_z(x,y)\hat{\mathbf{z}} \tag{10}$$

Contours of the flux function uniquely define the in-plane magnetic field. For a horizontal cut of the flux function $\Psi_{cut}(x)$ along the current sheet, the symmetry across the current sheet ensures that a local extremum in $\Psi_{cut}(x)$ corresponds to either a saddle point (x-line) or a local extremum (o-line) in $\Psi(x, y)$. For example, using the lower

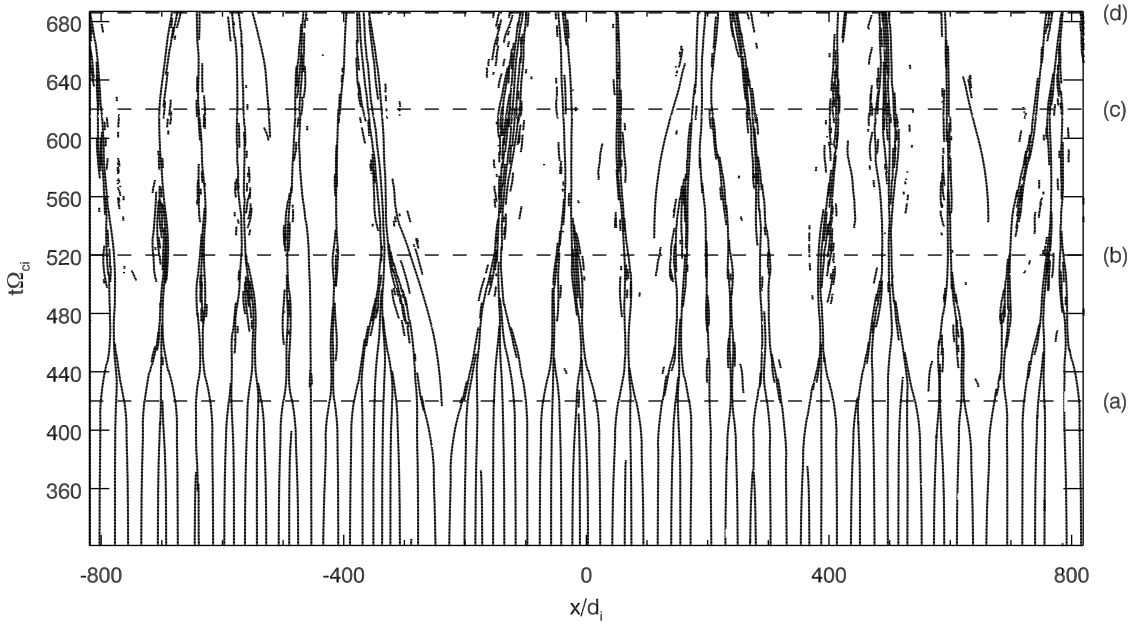

Figure 2. Location of all o-lines in time. Dashed lines correspond to snapshots of J_z in Figure 1.

current sheet in our simulations, the x-lines (o-lines) correspond to local minima (maxima) in $\Psi_{cut}(x)$. (Figure 2 tracks the positions of the o-lines according to this definition.) A magnetic island can now be defined by associating it with a particular x-line and a particular o-line. X-lines and o-lines are paired off by starting with the most highly embedded x-line, and after considering each of those o-lines that are located within its separatrices on both the left and the right, pairing it with the o-line that is closest in $\Psi_{cut}(x_{O,i})$. Figure 3a demonstrates this pairing scheme for a simple example. Note that defining islands in this way allows for islands to be contained entirely within other islands. This allows for a more realistic description of the merging process. If the x-line between the two islands is pushing the two islands apart, as in Figure 3b, this definition introduces a small error in that the lesser island (island A on the left, in green), despite being very nearly the same size as the dominant island (island B on the right, in red), has a border

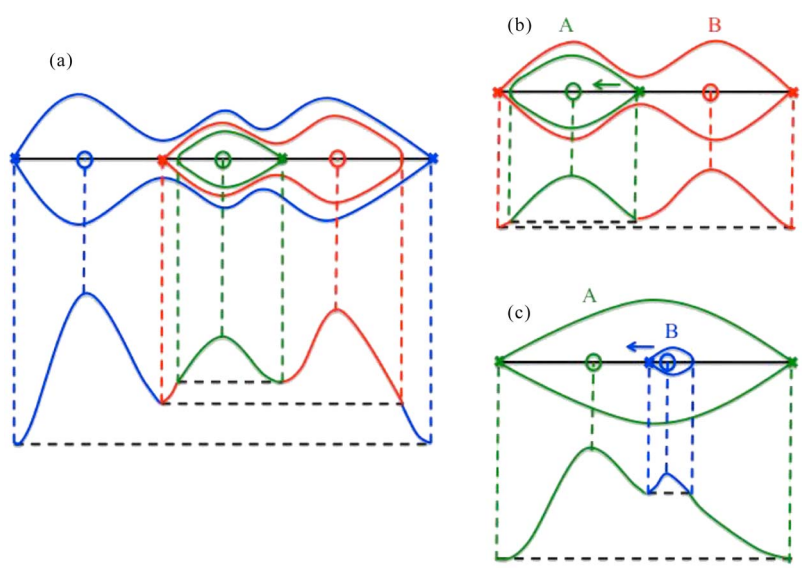

Figure 3. (a) A simple cartoon example of how magnetic islands can be defined by an x-line, o-line, and separatrix, all of the same color for a particular island. The corresponding $\Psi_{cut}(x)$ is shown below its current sheet, x-lines aligned with local minima and o-lines with local maxima. (b) A similar cartoon for two islands with a reconnecting x-line in between them pushing them apart. (c) Another example of two islands, now with a merging x-line in between. The lesser island shrinks as it is consumed by the dominant island.

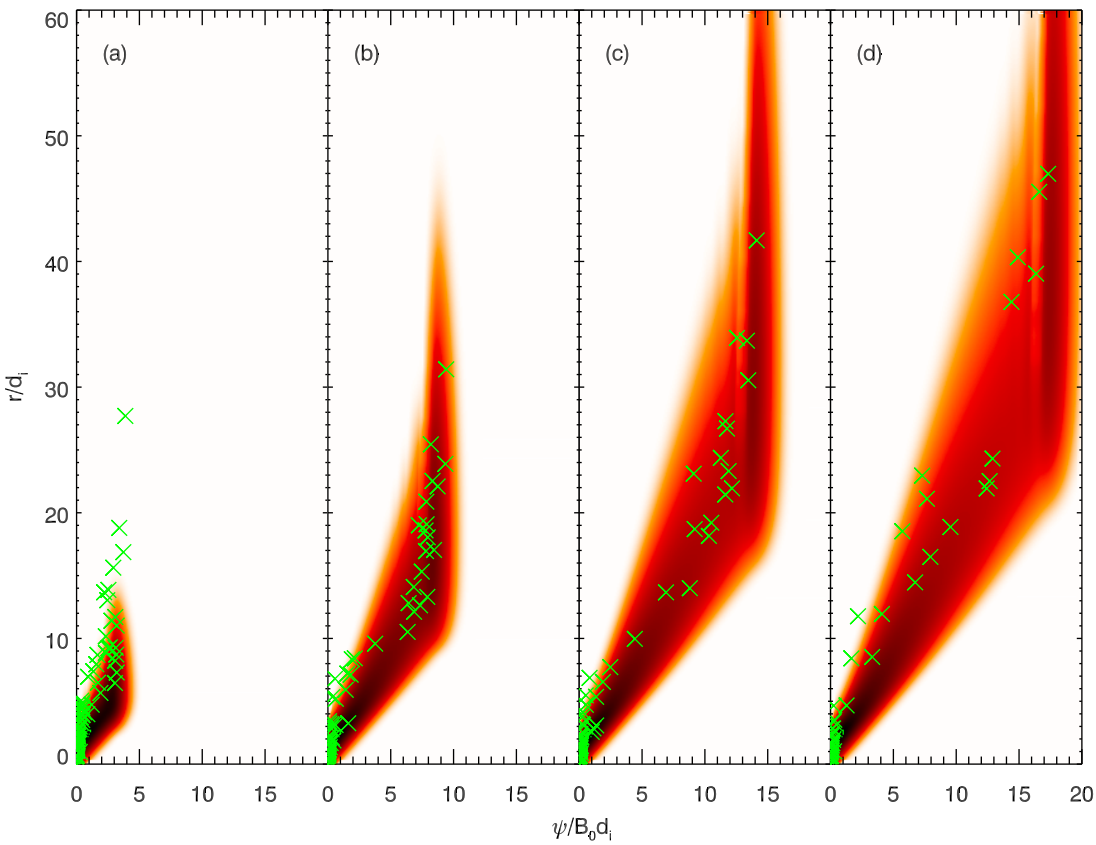

Figure 4. The distribution of islands in $\psi - r$ phase space in the Hall MHD simulation – each island is marked by a green x – overlaid on top of a numerical solution to equation (1) at times (a) $t = 420\Omega_{ci}^{-1}$, (b) $t = 520\Omega_{ci}^{-1}$, (c) $t = 620\Omega_{ci}^{-1}$, and (d) $t = 686\Omega_{ci}^{-1}$. See auxiliary material for an animated version of this figure.

which is completely within the dominant island. These two islands will both grow at similar rates, and their difference (signified by the region on the left surrounding island A but belonging to island B) becomes negligible compared to their overall size. On the other hand, if the two islands are merging with one another as in Figure 3c, then the size of the dominant island (island A, in green) steadily increases as it subsumes the lesser island (island B, in blue). Island B gradually shrinks until it is fully consumed by island A.

[17] Once all of the x-lines and o-lines have been paired off, then the flux ψ_i and area A_i of magnetic island i are simply given by

$$\psi_i = \Psi_{cut}(x_{O,i}) - \Psi_{cut}(x_{X,i}) \tag{11}$$

$$A_i = \int_{R_i} dA \tag{12}$$

where R_i is the region defined by the separatrix of the x-line for island i on the side which encompasses its o-line, but subtracting the regions of other islands entirely contained within R_i.

[18] Using this technique for any given time slice, each island can be plotted in the $\psi - r$ phase space as in Figure 4. The selected times correspond to the snapshots in Figure 1, with a green x corresponding to a particular magnetic island with flux ψ and characteristic radius r. (See auxiliary material for an animated version of Figure 4, where island trajectories in $\psi - r$ phase space can be seen more clearly.)[1] By following the trajectories of individual islands, we can see both mechanisms for island growth at play. During normal island growth (quasi-steady reconnection), an island's trajectory through the $\psi - r$ phase space in Figure 4 is generally along a diagonal with slope B_0 as reconnection injects flux into the island and consequently increases its area. Occasionally, a merger between two islands will push the dominant island off that diagonal into higher r, while not affecting its flux ψ. Meanwhile, the lesser island gravitates back towards the origin as it is consumed by the dominant one, losing both flux and area and eventually disappearing. The merging process therefore breaks the $\psi - r$ symmetry and allows islands to move above the symmetry diagonal $\psi = B_0 r$. The region below the symmetry diagonal in Figure 4 is prohibited since no mechanism exists for increasing the flux ψ without also proportionally increasing the scale size r. In other words, the model predicts an allowed region,

$$\psi < B_0 r \tag{13}$$

[1]Auxiliary materials are available in the HTML. doi:10.1029/2010JA016271.

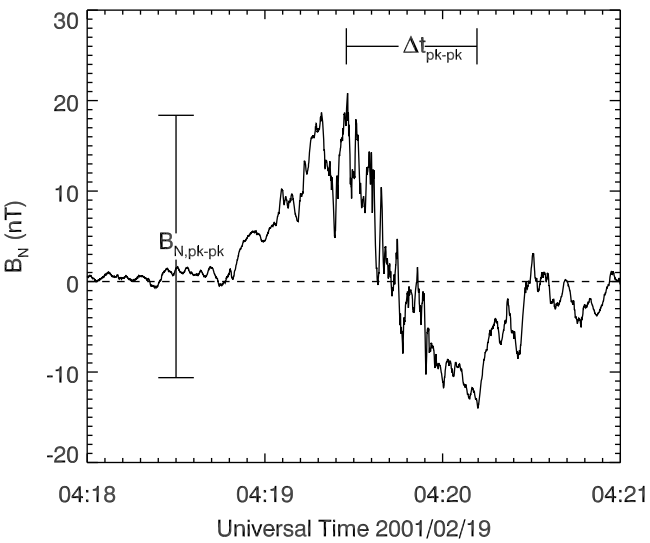

Figure 5. A sample flux transfer event observed by the four Cluster spacecraft at 0420 UT on 19 February 2001. The event occurred at (5.8, 4.7, 9.0)R_E in GSM coordinates.

that is consistent with all of the islands in the Hall MHD simulation.

[19] The results of the simulation allow us to study the two mechanisms for the growth of large islands by examining their trajectories in $\psi - r$ space and also to benchmark equation (1). Using the system size $L = 1638.4d_i$, we empirically match a numerical solution to equation (1) to determine appropriate values for the reconnection rate ε and the merging coefficient K_{mrg}. The quasi-steady reconnection rate ε governs the speed with which the distribution travels along the main diagonal $\psi = B_0 r$. In particular, since growth due to reconnection is the only mechanism that allows for growth in ψ, a simple empirical fit for $\dot{\psi} = \varepsilon c_A B_0$ yields ε. We can also fit the merging coefficient K_{mrg}, which controls the relative magnitudes of the merging and island growth terms and drives the $\psi - r$ asymmetry. We adjust K_{mrg} until the asymmetry of the numerical solution accounts for all of the islands in the Hall MHD simulation.

[20] Lastly, a non-trivial numerical solution to equation (1) requires a source of island creation. The rate of island creation in equation (1) is $S_N = \int_0^\infty dr \int_0^\infty d\psi S(\psi, r)$. However, since the Hall MHD simulations do not produce islands naturally, this method is not a reliable predictor for S_N in actual space plasmas. (Future PIC simulations may produce a better model for predicting this quantity.) The choice of S_N will instead reflect a value that generates a total number of islands $N(t) = \int_0^\infty dr \int_0^\infty d\psi f(\psi, r, t)$ consistent with the number of islands in the Hall MHD simulation exceeding some threshold flux $\psi_{\min} \approx 0.5 B_0 d_i$. Although most of the islands arise directly from the initial perturbation, rapid island growth $\propto \varepsilon$ proceeds only after an initial period of stagnation. Different islands reach this stage of growth at different times; only after starting its rapid growth phase do we count an island towards the total number of islands N. For most islands, this growth phase was in a roughly $60\Omega_{ci}^{-1}$ interval (between $370\Omega_{ci}^{-1}$ and $430\Omega_{ci}^{-1}$ in Figure 2).

[21] Choosing $S_N = 1.5\Omega_{ci}$, $\varepsilon = 0.055$, and $K_{mrg} = 6$ produces the numerical solution shown in red in both Figure 4. The fact that K_{mrg} is greater than unity emphasizes that merging plays an even more important role than was hypothesized by the original model in the study by *Fermo et al.* [2010]. The distributions of islands in the Hall MHD simulation (at the times of the panels shown in Figure 1) are overlaid on top of the numerical solution of equation (1) in red in Figure 4 as both evolve in time. The numerical solution is also shown in red in Animation S1, showing even more clearly the islands in the Hall MHD simulation and the numerical solution evolving synchronously. The distribution of islands follows the numerical solution quite well. The number of islands tracked in the simulation still is not enough to interpolate this data to a smooth distribution function, so this is still just a qualitative comparison. Nevertheless, the behavior of the islands in our Hall MHD simulation shows that equation (1) effectively describes island growth by quasi-steady reconnection (along the diagonal in $\psi - r$ phase space) and coalescence (adds to the characteristic radius r but not its flux ψ).

4. Cluster Observations of FTEs

[22] Flux transfer events (FTEs) were first identified by *Russell and Elphic* [1978] as flux ropes along the surface of the magnetopause, among the first observational evidence of reconnection. Their distinct signature was a magnetic field component normal to the magnetopause, B_N, which exhibits a bipolar signature. We equate them here with the magnetic islands seen in 2D simulations. Although flux tubes are inherently three-dimensional structures, Cluster observations of FTEs in 2006 show that they have a long azimuthal extent [*Fear et al.*, 2008], suggesting the feasibility of the two-dimensional picture of magnetic islands. The behavior of simulated FTEs in global MHD codes is consistent with that of the islands in our model. The FTEs form (generally near the subsolar region), grow, merge, and convect poleward until they are ejected into the cusps [*Omidi and Sibeck*, 2007]. We therefore treat the magnetopause as a single, very long current sheet with a length (south to north) of $L \sim 30R_E \sim 4000d_i$.

[23] Figure 5 shows a sample B_N profile for a flux transfer event. This data was taken from the ESA Cluster Active Archive, and also appeared in a study by *Wang et al.* [2005]. The FTE exhibits the characteristic bipolar signature in B_N of *Russell and Elphic* [1978]. This data was obtained from the fluxgate magnetotometer aboard Cluster spacecraft number 4 on a magnetopause crossing on 19 February 2001 at around 04:20 UT.

[24] During a three-year dayside phase of Cluster (2001–2003), the four spacecraft made many magnetopause crossings during which 1,098 flux transfer events (FTEs) were identified for a statistical study by *Wang et al.* [2005]. From each B_N profile and the plasma flow velocity, one can derive the approximate size of the FTE and the flux it contains. If the bipolar B_N signature is approximated by a sine wave, then we only need the time elapsed between peaks, Δt_{pk-pk}, the peak-to-peak magnitude of the B_N oscillation, BN, $pk{-}pk$, and the plasma flow speed v_{FTE}. Figure 5 shows how Δt_{pk-pk} and $B_{N,\ pk-pk}$ were calculated for the 19 February 2001 event. From these, a characteristic radius for the FTE can be calculated as $r = v_{FTE}\Delta t_{pk-pk}$, and its magnetic flux

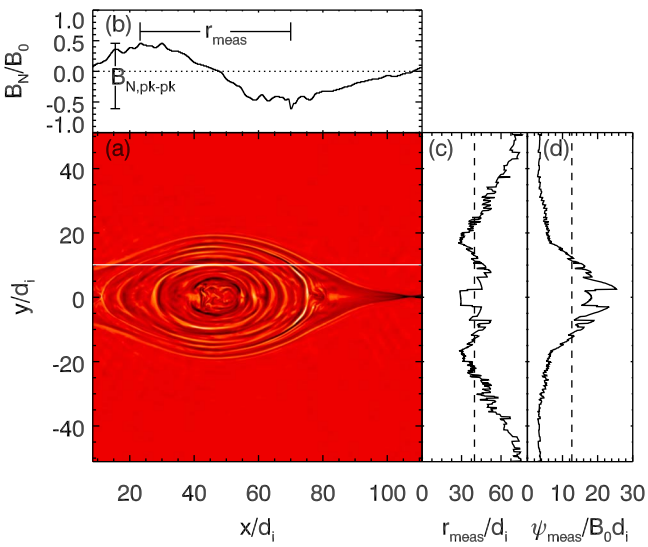

Figure 6. (a) J_z for a sample magnetic island from the Hall MHD simulation. (See Figure 1) (b) The bipolar B_N signature a spacecraft would measure from passing through this magnetic island traveling along the solid white horizontal line in Figure 6a, a distance $10d_i$ from the center of the main current sheet. To the right are (c) the scale size r_{meas} and (d) the magnetic flux ψ_{meas} that a spacecraft would measure by horizontally passing through the island a distance y from the current sheet. The dashed lines denote the actual scale size $r_{true} = (A_{true}/\pi)^{1/2}$ and magnetic flux ψ_{true}.

can be approximated by integrating half of the sine wave, $\psi = rB_{N,\ pk-pk}/\pi$.

[25] There are some limitations to this approach. In our model and in the simulations, the magnetic field is normalized to the asymptotic magnetic field upstream of the reconnection site B_0, but the FTEs in our database span three years and many different solar wind and magnetospheric conditions. Therefore, in order to make a valid comparison with the model's predictions, the magnetic field $B_{N,\ pk-pk}$ should be normalized to the reconnecting component of the tangential (to the magnetopause) magnetic field surrounding the FTE, $B_{t,\ surr}$. The quantity $B_{t,\ surr}$ obtained from Cluster, however, may include a guide field component, for which we cannot account. The magnetic field normalization might therefore be overestimated if guide field reconnection is occurring in the magnetopause. Determining the guide field requires knowledge of the flux rope orientation, which is itself a very difficult observational challenge. Another concern is that the database of FTEs provides one of the $B_{t,\ surr}$ values for either the magnetosheath or the magnetosphere side, depending on which side of the magnetopause that particular spacecraft was on when it encountered the FTE. The proper normalization requires $B_{t,\ surr}$ for both sides. (Of the 1,098 events, 730 of them measured $B_{t,\ surr}$ on the magnetosheath side.) For reconnection with asymmetric magnetic fields, the reconnection rate scales with the harmonic mean of the two upstream magnetic fields [*Cassak and Shay*, 2007]:

$$B_0 = \frac{2B_{sheath}B_{sphere}}{B_{sheath} + B_{sphere}}. \tag{14}$$

Since our database only provides either B_{sheath} or B_{sphere}, the proper normalization B_0 may vary from $B_{t,\ surr}$. After presenting the data we shall discuss the effect of these normalization questions.

[26] Another limitation to consider is the uncertainty of the proximity of the spacecraft's trajectory to the center of the FTE. The method prescribed here should be most accurate for a trajectory that goes straight through the center of the FTE along the surface of the magnetopause, and more prone to error farther away from the center of the FTE. In actuality though, it is the FTE that passes over the spacecraft. Cluster 4 was traveling at an average speed of about 2.3 km/s when the 19 February 2001 FTE in Figure 5 passed over the spacecraft, whereas the FTE flow velocity was measured as 186 km/s in a direction effectively along the surface of the magnetopause (within 9°). Consequently, the spacecraft trajectory through the FTE is essentially parallel to the magnetopause surface and corresponds to a horizontal cut through a magnetic island in our Hall MHD simulation.

[27] A typical island from the Hall MHD simulation performed in §3 is shown in Figure 6a. A spacecraft trajectory through the FTE at a distance $10d_i$ from the magnetopause surface (highlighted by a horizontal solid white line) would measure the bipolar B_N signature shown in Figure 6b. For this particular trajectory, r_{meas} is calculated from the peak-to-peak separation and ψ_{meas} from the peak-to-peak B_N. Performing this calculation for every horizontal cut across the magnetic island yields r_{meas} and ψ_{meas} as functions of y, the spatial separation between the trajectory and the current sheet. Both r_{meas} and ψ_{meas} are shown in Figure 6c and Figure 6d, respectively. The actual size r_{true} and flux ψ_{true} (determined as in §3.2) are displayed as dashed lines, for comparison. The measured values for both quantities are quite accurate when the trajectory passes through the island proper, even without going through the center. Far from the island, this method could overestimate the scale size and underestimate the flux, but in such cases where Cluster only passes by the outer edge of the FTE, the observed B_N profile will be weaker and generally more difficult to discern from the background noise. The signal-to-noise ratio is much lower in observational data such as Figure 5 than in MHD simulations such as in Figure 6b. Therefore, such events are less likely to be recognized as FTEs by Cluster and should not significantly skew the statistics.

[28] Other system parameters which could vary amongst different FTEs may also have an effect on island dynamics. For example, if plasma β, velocity shear, or T_i/T_e affects island formation (S_N), the nature of these effects are not yet firmly established. Their role is unaccounted for in this work, but could be of interest in future studies of island formation.

[29] The evolution equation, equation (1), normalizes length scales to εL. Direct measurements of the reconnection rate and magnetopause length are not possible, so in order to normalize the data properly, we approximate the numerical steady-state solution to equation (1) for the largest islands with an exponential tail for large r [*Fermo et al.*, 2010]:

$$\overline{F}_\infty(r) = \int_0^\infty d\psi F_\infty(\psi, r) \propto \exp(-r/r_0) \tag{15}$$

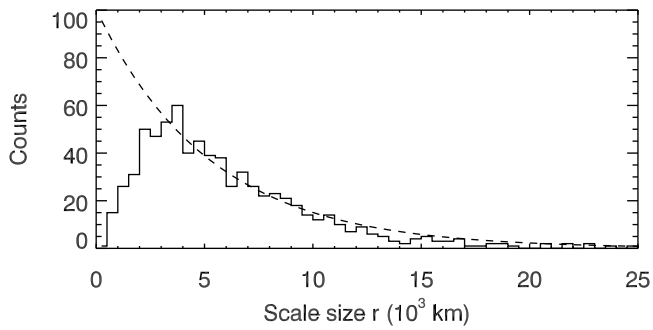

Figure 7. A distribution of the scale sizes of 1,098 flux transfer events detected by Cluster between 2001 and 2003. The dashed curve fits an exponential tail with r_0 = 5277 km to the tail of the distribution (beyond its peak).

with $r_0 = 2.64\varepsilon L$. Figure 7 shows that the distribution of FTEs in r agrees well with an exponential fit for r_0 = 5277 km. Equating these values for r_0, we estimate that $\varepsilon L \approx$ 2000 km. Using $L \approx 30R_E$ for the magnetopause, one can also indirectly estimate the average reconnection rate to be $\varepsilon \approx 0.01$.

[30] Figure 8a shows most of the 1,098 flux transfer events accordingly normalized. (Two events with ψ or r outside of the box are excluded.) These data points are overlaid on a steady-state numerical solution to equation (1) with normalized source amplitude $S_N^* = S_N\varepsilon L/c_A = 4000$ and merging coefficient $K_{mrg} = 6$. Qualitatively, the distribution of FTEs compares favorably with that predicted by the model, in that the distribution of islands appears to exhibit behavior consistent with island growth due to quasi-steady reconnection (along the symmetry diagonal) and merging (northward in phase space). The large majority of the FTEs observed by Cluster fall into the region above the $\psi = B_{t,\ surr}r$ diagonal, as described by equation (13).

[31] The 52 outliers below the diagonal (in red) have $\psi_{meas} > B_{t,\ surr}r_{meas}$. To account for these outliers, Figure 8b shows the average in-plane magnetic field within the FTE $\psi_{meas}/B_{t,\ surr}r_{meas}$ versus $B_{t,\ surr}$. The 52 outliers below the diagonal were normalized to a comparatively small $B_{t,\ surr}$, almost all less than the mean $B_{t,\ surr}$ of 23.4 nT. Furthermore, 42 out of the 52 outliers (or 81%) measured $B_{t,\ surr}$ in the magnetosheath, where typically $B_{sheath} < B_{sphere}$. Recall, however, that the proper normalization for the magnetic field should have accounted for B_t both in the magnetosheath and in the magnetosphere. When the measured $B_{t,\ surr}$ is quite small, it is quite likely that B_t is larger on the other side of the magnetopause. If this is the case, then equation (14) dictates that $B_0 > B_{t,\ surr}$ by as much as a factor of two. Although the data necessary to make this correction are not available, the fact that all of the outliers have low $B_{t,\ surr}$ suggests that the proper normalization could push many of those outliers back into the allowed region described by equation (13). On the other hand, if guide field reconnection is occurring, the presence of a guide field would have the opposite effect, since $B_{t,\ surr}$ would include the guide field component as well as B_0. Further observational work can be done to ascertain the guide field and magnetic field asymmetry in these events to obtain the current normalization for the magnetic fields.

[32] Normalization issues notwithstanding, the strong asymmetry in $\psi - r$ phase space indicates that, as in the Hall MHD simulations, merging is a very prominent factor in island dynamics. Yet for merging to play a significant role, very many islands must be present at any given time. This suggests that reconnection is quite patchy at the magnetopause. Furthermore, the bulk of these islands will be quite small, perhaps too small for spacecraft instrumentation to resolve or to distinguish from noise. A large, detailed statistical study of FTEs such as that performed by *Wang et al.* [2005] is likely to miss the preponderance of FTEs at small scales. Even assuming a simple linear tearing mode that produces FTEs typically with $k\lambda \sim 1$ (where $\lambda \sim d_i \sim 50$ km is the current sheet width) yields islands as small as $2\pi/k \sim 2\pi\lambda \sim 300$ km. Therefore, the precipitous dropoff in FTEs smaller than roughly 4000 km in Figure 7 probably does not

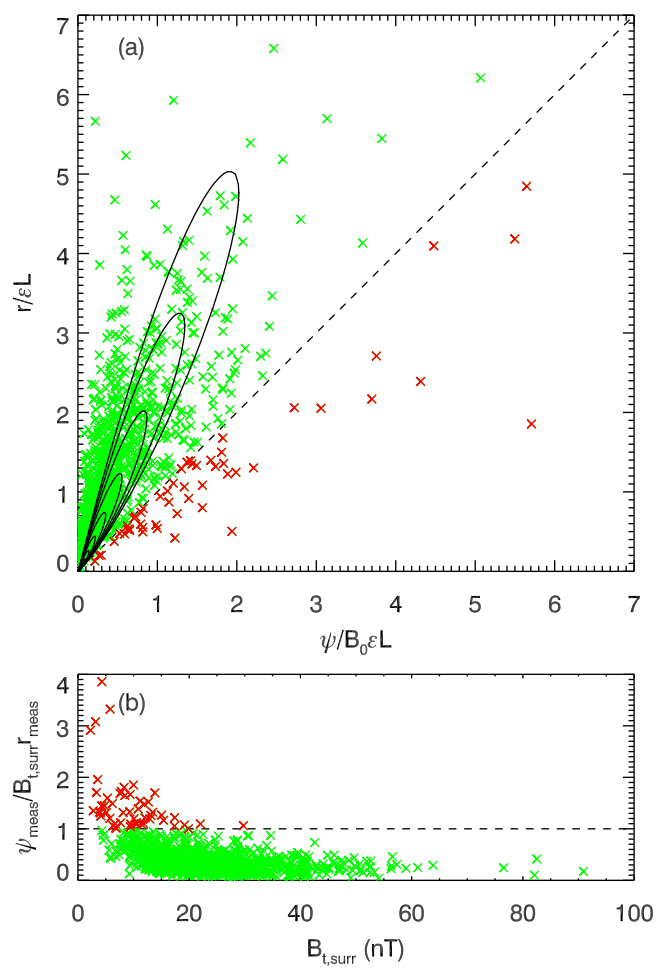

Figure 8. (a) The distribution of flux transfer events in $\psi - r$ phase space, overlaid on a numerical steady-state solution to equation (1) for appropriate parameters. Flux transfer events above the $\psi = B_0r$ diagonal are in green, whereas those in the prohibited region below the diagonal are marked in red. (b) The (normalized) average in-plane magnetic field within the FTE versus the absolute (non-normalized) $B_{t,surr}$. The horizontal dashed line corresponds to the diagonal dashed line of Figure 8a. Most of the outlier events have small $B_{t,surr}$.

paint the whole picture, since any generation mechanism of FTEs must have them starting out much smaller than 4000 km. A more likely scenario for Figure 7 is that FTEs at small scales are actually much more numerous than those which can be observed by the spacecraft.

5. Conclusions

[33] We have developed a statistical model for magnetic islands in very long current layers that is consistent with both Hall MHD simulations and Cluster FTE observations. Using Hall MHD simulations, we have explored the mechanisms for the growth of large-scale magnetic islands. The trajectories of islands in a space defined by its characteristic radius and flux reveal that islands grow by (1) quasi-steady reconnection (adding both area and flux), and (2) merging (adding area but not flux). We have also used the Hall MHD simulations to benchmark the model by fitting the model parameters to the results of the simulation. In particular, the result that $K_{mrg} \approx 6$ in our simulations underscores the importance of merging in very large systems.

[34] Observations of flux transfer events from the four Cluster spacecraft are also consistent with the predictions of the model. The islands in the Hall MHD simulation and the FTEs observed by Cluster show good qualitative agreement with the predicted distributions of islands. More particularly, the preponderance of these islands reside in the allowed region predicted by equation (13). This is further evidence that island merging plays a significant role in the dynamics of long current layers. In this scenario, patchy reconnection generates many islands, most of which are smaller than the resolving capabilities of most spacecraft instruments. Spacecraft are only recently starting to see secondary island structures at small scales; for example, [*Teh et al.*, 2010] have recognized a secondary magnetic island within the Hall quadrupolar field region in a THEMIS magnetopause crossing, and the MMS (Magnetospheric Multiscale) mission will further explore these scales. Nonetheless, to this point structures of this size are very difficult to see in observations or simulate in models.

[35] Continued work addressing the validation of this model is still possible. A Hall MHD simulation which generates islands spontaneously and convects those islands outwards towards an open boundary would allow for a more direct comparison with our model. Additional observational work with the Cluster data accounting for the possibility of a guide field and for magnetopause asymmetry would increase confidence in the magnetic field normalizations.

[36] A better understanding of the generation mechanism for magnetic islands (and consequently of the source term S_N) is also highly desirable. The conditions for island formation and the effects of system parameters such as plasma β, velocity shear, or T_i/T_e, remain poorly understood. The results of the present study point towards PIC simulations as the preferred method. Global fluid simulations of the magnetopause, which often show at most a few FTEs at a time [*Raeder*, 2006; *Dorelli and Bhattacharjee*, 2009], might lack the resolution to see the small-scale FTEs generated at kinetic scales. Recent attempts at global hybrid simulations can explore some of these dynamics, but are still much smaller than actual system sizes, and still lack some potentially important physics (e.g., electron inertia) [*Omidi and Sibeck*, 2007].

[37] We can also follow up the observations of FTEs described here with observations of magnetic islands in other systems besides the magnetopause. Similar structures have been observed in the magnetotail [*Chen et al.*, 2008], but to our knowledge no sizable database of islands has been compiled there. In solar flares, supra-arcade downflows [*Sheeley et al.*, 2004; *Linton and Longcope*, 2006] have been identified as magnetic flux tubes. A quantitative study of these coronal structures has already produced statistical distributions characterizing them by their size and their flux [*McKenzie and Savage*, 2009]. Provisional comparisons of these distributions with those predicted by this model are encouraging, in that they appear to also exhibit an exponential tail [*Savage*, 2010; S. L. Savage, private communication, 2010]. However, the limited resolution of TRACE and SXT images hinders the proper separation of scales, and a more extensive study with larger data sets would prove more useful in the validation of this model. In particular, the new Solar Dynamics Observatory (SDO) mission promises high-resolution images of solar flares. A similar examination as performed by *McKenzie and Savage* [2009] using SDO images would enable a quantitative comparison with this model.

[38] **Acknowledgments.** The authors would like to thank Yongli Wang at the NASA Goddard Space Flight Center for helpful conversations and for generously sharing the FTE database he compiled. This work was supported by NASA through the Earth and Space Science Fellowship NNX07A083H and NNX09A102G. Computations were performed at the National Energy Research Scientific Computing Center. Spacecraft data from Cluster was obtained from the ESA Cluster Active Archive.

[39] Philippa Browning thanks the reviewers for their assistance in evaluating this paper.

References

Angelopoulos, V., et al. (1995), Growth and evolution of a plasmoid associated with a small, isolated substorm: IMP 8 and GEOTAIL measurements in the magnetotail, *Geophys. Res. Lett.*, *22*(22), 3011–3014.

Bhattacharjee, A., Y.-M. Huang, H. Yang, and B. Rogers (2009), Fast reconnection in high-Lundquist-number plasmas due to the plasmoid instability, *Phys. Plasmas*, *16*, 112102.

Birn, J., M. Hesse, and K. Schindler (1996), MHD simulations of magnetotail dynamics, *J. Geophys. Res.*, *101*(A6), 12,939–12,954.

Birn, J., et al. (2001), Geospace Environmental Modeling (GEM) Magnetic Reconnection Challenge, *J. Geophys. Res.*, *106*, 3715.

Biskamp, D. (1986), Magnetic reconnection via current sheets, *Phys. Fluids*, *29*, 1520.

Cassak, P., and M. A. Shay (2007), Scaling of asymmetric magnetic reconnection: General theory and collisional simulations, *Phys. Plasmas*, *14*, 102114.

Cassak, P. A., M. A. Shay, and J. F. Drake (2009), Scaling of Sweet-Parker reconnection with secondary islands, *Phys. Plasmas*, *16*, 120702.

Chen, L.-J., et al. (2008), Observation of energetic electrons within magnetic islands, *Nat. Phys.*, *4*, 19–23.

Dailey, R., C. A. Cattell, F. S. Mozer, and J. Berchem (1985), Electric fields and convection velocities associated with flux transfer events, *Geophys. Res. Lett.*, *12*(12), 843–846.

Daughton, W., H. Karimabadi, and J. Scudder (2006), Fully kinetic simulations of undriven magnetic reconnection with open boundary conditions, *Phys. Plasmas*, *13*, 072,101.

Daughton, W., V. Roytershteyn, B. J. Albright, H. Karimabadi, L. Yin, and K. J. Bowers (2009), Transition from collisional to kinetic regimes in large-scale reconnection layers, *Phys. Rev. Lett.*, *103*, 065004.

Dorelli, J. C., and A. Bhattacharjee (2009), On the generation and topology of flux transfer events, *J. Geophys. Res.*, *114*, A06213, doi:10.1029/2008JA013410.

Dorelli, J. C., and J. Birn (2001), Electron magnetohydrodynamic simulations of magnetic island coalescence, *Phys. Plasmas*, *8*(9), 4010.

Drake, J. F., M. Swisdak, K. M. Schoeffler, B. N. Rogers, and S. Kobayashi (2006a), Formation of secondary islands during magnetic reconnection, *Geophys. Res. Lett.*, *33*, L13105, doi:10.1029/2006GL025957.

Drake, J. F., M. Swisdak, H. Che, and M. A. Shay (2006b), Electron acceleration from contracting magnetic islands during reconnection, *Nature*, *443*, 553.

Eastwood, J. P., et al. (2007), Multi-point observations of the Hall electromagnetic field and secondary island formation during magnetic reconnection, *J. Geophys. Res.*, *112*, A06235, doi:10.1029/2006JA012158.

Egedal, J., A. Lê, Y. Zhu, W. Daughton, M. Øieroset, T. Phan, R. P. Lin, and J. P. Eastwood (2010), Cause of super-thermal electron heating during magnetotail reconnection, *Geophys. Res. Lett.*, *37*, L10102, doi:10.1029/2010GL043487.

Elphic, R. C., C. A. Cattell, K. Takahashi, S. J. Bame, and C. T. Russell (1986), ISEE-1 and 2 observations of magnetic flux ropes in the magnetotail: FTE's in the plasma sheet?, *Geophys. Res. Lett.*, *13*(7), 648–651.

Farrugia, C. J., et al. (1988), A multi-instrument study of flux transfer event structure, *J. Geophys. Res.*, *93*(A12), 14,465–14,477.

Fear, R. C., S. E. Milan, A. N. Fazakerley, E. A. Lucek, S. W. H. Cowley, and I. Dandouras (2008), The azimuthal extent of three flux transfer events, *Ann. Geophys.*, *26*, 2353–2369.

Fermo, R. L., J. F. Drake, and M. Swisdak (2010), A statistical model of magnetic islands in a current layer, *Phys. Plasmas*, *17*, 010702.

Finn, J. M., and P. K. Kaw (1977), Coalescence instability of magnetic islands, *Phys. Fluids*, *20*, 72.

Fujimoto, K. (2006), Time evolution of the electron diffusion region and the reconnection rate in fully kinetic and large system, *Phys. Plasmas*, *13*, 072904.

Furth, H. P., J. Killeen, and M. N. Rosenbluth (1963), Finite-resistivity instabilities of a sheet pinch, *Phys. Fluids*, *6*(4), 459.

Hesse, M., and J. Birn (1991), Plasmoid evolution in an extended magnetotail, *J. Geophys. Res.*, *96*(A4), 5683–5696.

Huang, Y.-M., and A. Bhattacharjee (2010), Scaling laws of resistive magnetohydrodynamic reconnection in the high-Lundquist-number, plasmoid-unstable regime, *Phys. Plasmas*, *17*(6), 062104.

Karimabadi, H., W. Daughton, and J. Scudder (2007), Multi-scale structure of the electron diffusion region, *Geophys. Res. Lett.*, *34*, L13104, doi:10.1029/2007GL030306.

Klimas, A., M. Hesse, and S. Zenitani (2008), Particle-in-cell simulation of collisionless reconnection with open outflow boundaries, *Phys. Plasmas*, *15*, 082102.

Lapenta, G. (2008), Self-feeding turbulent magnetic reconnection on macroscopic scales, *Phys. Rev. Lett.*, *100*, 235001.

Lee, L. C., and Z. F. Fu (1985), A theory of magnetic flux transfer at the earth's magnetopause, *Geophys. Res. Lett.*, *12*, 105.

Lin, J., Y.-K. Ko, L. Sui, J. C. Raymond, G. A. Stenborg, Y. Jiang, S. Zhao, and S. Mancuso (2005), Direct observations of the magnetic reconnection site of an eruption on 2003 November 18, *Astrophys. J.*, *622*, 1251–1264.

Linton, M. G., and D. W. Longcope (2006), A model for patchy reconnection in three dimensions, *Astrophys. J.*, *642*, 1177–1192.

Loureiro, N. F., A. A. Schekochihin, and S. Cowley (2007), Instability of current sheets and formation of plasmoid chains, *Phys. Plasmas*, *14*, 100703.

McKenzie, D. E., and S. L. Savage (2009), Quantitative examination of supra-arcade downflows in eruptive solar flares, *Astrophys. J.*, *697*, 1569–2009.

Omidi, N., and D. G. Sibeck (2007), Flux transfer events in the cusp, *Geophys. Res. Lett.*, *34*, L04106, doi:10.1029/2006GL028698.

Pritchett, P. L., and C. C. Wu (1979), Coalescence of magnetic islands, *Phys. Fluids*, *22*(11), 2140–2146.

Raeder, J. (2006), Flux tranfer events: 1. Generation mechanism for nearly southward IMF, *Ann. Geophys.*, *24*, 381.

Russell, C. T., and R. C. Elphic (1978), Initial isee magnetometer results: Magnetopause observations, *Space Sci. Rev.*, *22*, 681.

Samtaney, R., N. F. Loureiro, D. A. Uzdensky, A. A. Schekochihin, and S. C. Cowley (2009), Formation of plasmoid chains in magnetic reconnection, *Phys. Rev. Lett.*, *103*, 105004.

Savage, S. L. (2010), Using extreme ultra-violet and soft X-ray observations as probes of magnetic reconnection during solar flares, Ph.D. thesis, Mont. State Univ., Bozeman, Mont.

Shay, M. A., J. F. Drake, M. Swisdak, and B. N. Rogers (2004), The scaling of embedded collisionless reconnection, *Phys. Plasmas*, *11*(5), 2199.

Shay, M. A., J. F. Drake, and M. Swisdak (2007), Two-scale structure of the electron dissipation region during collisionless magnetic reconnection, *Phys. Rev. Lett.*, *99*, 155002.

Sheeley, N. R., H. P. Warren, and Y.-M. Wang (2004), The origin of post-flare loops, *Astrophys. J.*, *616*, 1224.

Shepherd, L. S., and P. A. Cassak (2010), Comparison of secondary islands in collisional reconnection to hall reconnection, *Phys. Rev. Lett.*, *105*, 015004.

Shibata, K., and S. Tanuma (2001), Plasmoid-induced-reconnection and fractal reconnection, *Earth Planets Space*, *53*, 473–482.

Slavin, J. A., M. F. Smith, E. L. Mazur, D. N. Baker, E. W. Hones Jr., T. Iyemori, and E. W. Greenstadt (1993), ISEE 3 observations of traveling compression regions in the Earth's magnetotail, *J. Geophys. Res.*, *98*(A9), 15,425–15,446.

Slavin, J. A., et al. (2003), Geotail observations of magnetic flux ropes in the plasma sheet, *J. Geophys. Res.*, *108*(A1), 1015, doi:10.1029/2002JA009557.

Teh, W.-L., S. E. B. U. O. Sonnerup, R. Ergun, V. Angelopoulos, K.-H. Glassmeier, J. P. McFadden, and J. W. Bonnell (2010), THEMIS observations of a secondary magnetic island within the hall electromagnetic field region at the magnetopause, *Geophys. Res. Lett.*, *37*, L21102, doi:10.1029/2010GL045056.

Uzdensky, D. A., and J. Goodman (2008), Statistical description of a magnetized corona above a turbulent accretion disk, *Astrophys. J.*, *682*(1), 608–629.

Uzdensky, D. A., N. F. Loureiro, and A. A. Schekochihin (2010), Fast magnetic reconnection in the plasmoid-dominated regime, *Phys. Rev. Lett.*, *105*(23), 235002.

Wang, Y. L., et al. (2005), Initial results of high-latitude magnetopause and low-latitude flank flux transfer events from 3 years of Cluster observations, *J. Geophys. Res.*, *110*, A11221, doi:10.1029/2005JA011150.

J. F. Drake, R. L. Fermo, and M. Swisdak, Institute for Research in Electronics and Applied Physics, University of Maryland, College Park, MD 20742-3511, USA. (rfermo@umd.edu)

K.-J. Hwang, NASA Goddard Space Flight Center, Greenbelt, MD 20771, USA.